


Speciation and precipitation of heavy metals in high-metal and high-acid mine waters from the Iberian Pyrite Belt (Portugal)

Nuno Durães¹  · Iuliu Bobos² · Eduardo Ferreira da Silva¹

Received: 4 March 2016 / Accepted: 28 November 2016 / Published online: 12 December 2016
© Springer-Verlag Berlin Heidelberg 2016

Abstract Acid mine waters (AMW) collected during high- and low-flow water conditions from the Lousal, Aljustrel, and São Domingos mining areas (Iberian Pyrite Belt) were physicochemically analyzed. Speciation calculation using PHREEQC code confirms the predominance of Me^{n+} and Me-SO_4 species in AMW samples. Higher concentration of sulfate species (Me-SO_4) than free ion species (Me^{n+} , i.e., Al, Fe, and Pb) were found, whereas opposite behavior is verified for Mg, Cu, and Zn. A high mobility of Zn than Cu and Pb was identified. The sulfate species distribution shows that $\text{Fe}^{3+}\text{-SO}_4^{2-}$, SO_4^{2-} , HSO_4^- , Al-SO_4 , MgSO_4^0 , and CaSO_4^0 are the dominant species, in agreement with the simple and mixed metal sulfates and oxy-hydroxysulphates precipitated from AMW. The saturation indices (SI) of melanterite and epsomite show a positive correlation with Cu and Zn concentrations in AMW, which are frequently retained in simple metal sulfates. Lead is well correlated with jarosite and alunite (at least in very acid conditions) than with simple metal sulfates. The Pb for K substitution in jarosite occurs as increasing Pb concentration in solution. Lead mobility is also controlled by anglesite precipitation (a fairly insoluble sulfate), where a

positive correlation was ascertained when the SI approaches equilibrium. The zeta potential of AMW decreased as pH increased due to colloidal particles aggregation, where water species change from SO_4^{2-} to OH^- species during acid to alkaline conditions, respectively. The AMW samples were supersaturated in schwertmannite and goethite, confirmed by the $\text{Me}^{n+}\text{-SO}_4$, $\text{Me}^{n+}\text{-Fe-O-OH}$, or $\text{Me}^{n+}\text{-S-O-Fe-O}$ complexes identified by attenuated total reflectance infrared spectroscopy (ATR-IR). The ATR-IR spectrum of an AMW sample with pH 3.5 (sample L1) shows well-defined vibration plans attributed to SO_4 tetrahedron bonded with Fe-(oxy)hydroxides and the Me^{n+} sorbed by either SO_4 or Fe-(oxy)hydroxides. For samples with lower pH values (pH ~ 2.5—samples SD1 and SD4), the vibration plans attributed to Me^{n+} sorption are not evidenced, indicating its release in solution. The sorption of heavy metals on the first precipitated simple metal sulfates was ascertained by scanning electron microscopy coupled with X-ray spectrometry (SEM-EDX), where X-ray maps of Cu and Zn confirm a distribution of both metals in the melanterite structure.

Keywords Acid mine waters · Heavy metals · Metal speciation · Sulfates · Zeta potential · Infrared spectroscopy · Electron microscopy · Iberian Pyrite Belt

Responsible editor: Philippe Garrigues

✉ Nuno Durães
nunoduraes@ua.pt

¹ Departamento de Geociências da Universidade de Aveiro. GeoBioTec – Geobiociências, Geotecnologias e Geoengenharia, Campus de Santiago, 3810-193 Aveiro, Portugal

² Departamento de Geociências, Ambiente e Ordenamento do Território, Faculdade de Ciências da Universidade do Porto. ICT – Instituto de Ciências da Terra, Rua do Campo Alegre 687, 4169-007 Porto, Portugal

Introduction

The acid mine drainage (AMD) is one of most severe impacts associated with mining operations, which has high-cost liabilities (Lottermoser 2007). The AMD is generated by both biotic and abiotic sulfide oxidation, releasing high amounts of sulfuric acid and metals into surface and ground waters (Jambor and Blowes 1998; Nordstrom and Alpers 1999; Carvotta 2008). A decrease in AMD contamination can be

observed in time (Lambert et al. 2004), but the problems may persist for a long period, even after mining has ceased (Lottermoser 2007). This is particularly marked in highly acidic waters ($\text{pH} < 3.5$), where metal contamination is slowly attenuated, expressing the similar element ratios of the primary minerals from which they were released (Nordstrom 2011).

The ability for acid generation is not the same for sulfide minerals. The oxidation of monosulfides (e.g., galena, sphalerite, arsenopyrite) by O_2 does not lead to a direct acid production (Jennings et al. 2000; Weisener et al. 2004; Walker et al. 2006; Yunmei et al. 2007). By contrast, when the oxidation of disulfides (e.g., pyrite, pyrrhotite) by O_2 takes place, the H^+ is released in solution (Nordstrom 1982; Nicholson and Schärer 1994). Otherwise, the Fe^{3+} is a strong oxidant, which may produce more acidity than by O_2 mediation (Singer and Stumm 1970; Nordstrom 1982; Rimstidt et al. 1994; Stumm and Morgan 1996; Janzen et al. 2000; Yunmei et al. 2007; McKibben et al. 2008). The Fe^{2+} oxidation rates by O_2 in neutral to alkaline conditions are higher than in acid conditions, where the precipitation of Fe(III)-oxyhydroxides coat the sulfide minerals, reducing the reactive surface and inhibiting the oxidation process. At low pH, the oxidation rate of Fe^{2+} to Fe^{3+} is lower than the rate of Fe^{3+} reduction by pyrite (Singer and Stumm 1970). Other way, the presence of acidophilic bacteria causes the acceleration of the oxidation of Fe^{2+} , where the Fe^{3+} ($\text{pH} < 3$) is the only effective oxidizer of pyrite (Singer and Stumm 1970; Nordstrom 1982). Also, due to the higher proportion of pyrite regarding other sulfides in tailings impoundments or waste dumps, this mineral is the one of most concern in AMD production.

Once sulfides oxidation started, the highly acidic conditions generated will promote the dissolution of other mineral phases, and a high concentration mixing pool of elements will persist in the aqueous system. Thus, the physicochemical conditions and the interactions between the metal(loid)s and complexing ligands will control the speciation and the solubility/precipitation of metal(loid)s in acid mine waters (AMW).

Different aqueous species are distinguishable energetically, stoichiometrically, and structurally (Stumm and Morgan 1996), allowing changes of kinetic, thermodynamic properties, solubility, and toxicity (Millero 2001). Speciation that determines, at certain extent, the metal complexation and precipitation will influence its bioavailability and hazards (Simpson et al. 2014).

The Al and Fe are two of the most abundant cations in AMW, where changes in the physicochemical parameters (i.e., pH, ionic strength, and temperature) can lead to formation of Al and Fe precipitates with high surface area, low crystallinity (Bigham et al. 1996; Bigham and Nordstrom

2000) and high sorption ability for metal(loid)s (Dzombak and More 1990; Stumm and Morgan 1996; Bigham and Nordstrom 2000). Likewise, SO_4^{2-} is the most important anion in AMD, which may form complexes with Fe and Al and precipitate. Many of these sulfates or oxy-hydroxysulfates (where a significant amount of metal(loid)s are adsorbed or co-precipitated) are highly soluble and easily released those metal(loid)s again to the waters during the first rain events, making the aqueous system more acidic (Alpers et al. 1994; Kimball 1994; Nordstrom and Alpers 1999; Jambor et al. 2000; Jerz and Rimstidt 2003; Hammarstrom et al. 2005; Sánchez España et al. 2005; Romero et al. 2006; Sánchez España et al. 2006; Nordstrom 2009).

The Iberian Pyrite Belt (IPB) has a long mining history, where a large number of mines with similar ore genesis and mineralogical composition are affected by AMD, making this an attractive site for the study of aqueous geochemical processes.

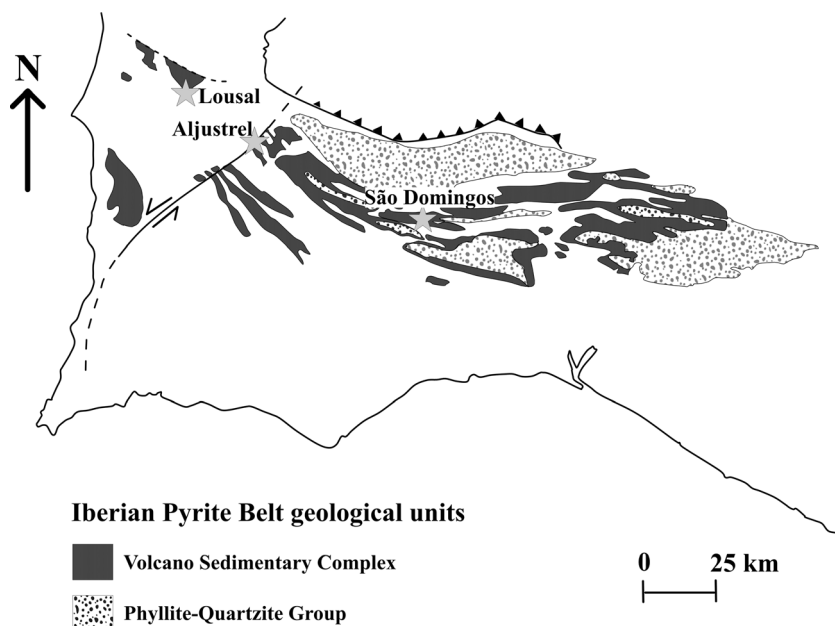
The main goal proposed in this study was to evaluate and compare the behavior of the metals (Al, Cu, Fe, Mg, Pb, and Zn) in high-metal and high-AMW across the IPB (Aljustrel, Lousal and São Domingos mines). The distribution of dissolved species and saturation indices for the most common minerals precipitated from AMW were calculated for all samples collected. Additionally, the complexation type of metals was studied by infrared spectroscopy, and the sorption of metals on the first precipitated sulfates was ascertained by electron microscopy.

Geological background

The IPB metallogenic province is recognized for its volcanogenic massive sulfides type mineralization, which extends about 230 km from the vicinity of western Portuguese coast close to Seville (Spain), ranging from 30 to 60 km in width (Fig. 1). The massive sulfide ores and also some Mn mineralization occur in the volcano-sedimentary complex (Schermerhorn 1971; Carvalho et al. 1976; Barriga et al. 1997), ranging from Devonian to Carboniferous (Late Famennian to Late Viséan) ages (Oliveira et al. 2004).

The Lousal mine is formed by 18 mineralized sulfide lenses, mainly composed of pyrite, probably belonging to the same ore body affected by folding and faults that caused its segmentation (Matzke 1971). The Aljustrel ore deposit comprises six sulfide masses displayed in three main parallel alignments, where pyrite, sphalerite, galena, antimony, sulfosalts, tin minerals, and arsenopyrite occur (Andrade and Schermerhorn 1971; Barriga 1983; Barriga and Fyfe 1988; Gaspar 1996; Barriga and Fyfe 1998). The São Domingos mine is characterized by a unique pyritic body with variable amounts of chalcopyrite, sphalerite, and galena (Webb 1958;

Fig. 1 Simplified geological map of Iberian Pyrite Belt (adapted from Carvalho et al. 1976). Location of the Lousal, Aljustrel, and São Domingos study mining areas



Carvalho 1971), where a huge gossan overlying the mineralization occurs at the surface.

Materials and methods

Sampling sites location

The AMW samples from Aljustrel (A), Lousal (L), and São Domingos (SD) (Fig. 2a–c) were collected, such as artificial dams used for collection and treatment of the drained waters directly from the underground mines, open-pits, tailings impoundments, a decantation tank used for Cu precipitation in the past (Aljustrel), and streams affected by AMD.

Two sampling periods (wet and dry season) were chosen to collect samples from the Aljustrel mining area and only one sampling period (dry season) was chosen for the sample collection from the Lousal and São Domingos mining areas, in order to ascertain the variations of the physicochemical parameters and the chemical concentration.

The water samples were collected in acid-rinsed polyethylene bottles and stored refrigerated during transport to the laboratory. The physicochemical parameters (pH, temperature, and electric conductivity (EC)) were measured in field and then in laboratory using a HI-255 multiparameter from HANNA Instruments® with a HI-1131B combined glass electrode for pH measurements and a HI-76310 probe for EC determination. Both pH and EC electrodes were previously calibrated with a two-point buffer standard solution (pH 4.01 and 7.01) and a one-point standard solution ($1413 \mu\text{S cm}^{-1}$), respectively. The specific conductance (SC)

values were obtained through the correction of EC values by the electrical conductivity temperature compensation method proposed by McCleskey (2013).

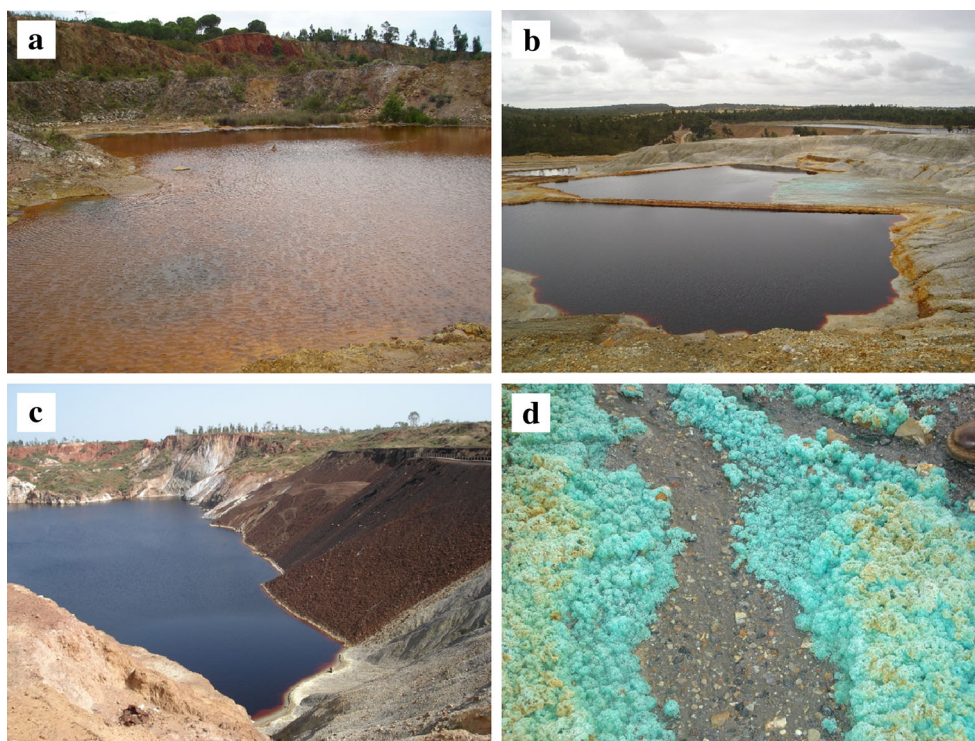
Water samples were filtered in the laboratory under vacuum through $0.45 \mu\text{m}$ pore size Millipore filters (no more than 24 h pass between the water collection and filtration). Three subsamples were separated: one non-acidified for sulfate determination, another acidified (pH < 2) with ultra-pure HNO_3 (to prevent metals precipitation) for cations and Cl determination, and another acidified with ultra-pure HCl for Fe(II) determination. All samples were stored in a refrigerator at 4°C until analyses performance.

Efflorescence samples were collected from the surface of the tailings impoundments and from the edges of the open-sites with AMW, where the efflorescences precipitate during the water evaporation (Fig. 2d).

Analytical techniques

The chemical analyses of waters were carried out by inductive-coupled plasma mass spectrometry (ICP-MS) at the ACME Labs (ACME Anal. ISO 9002 Accredited Lab, Canada), followed a rigorous quality program, which included the use of certified reference materials (STANDARD WASTWATERD9), reagent blanks, and duplicate samples. The detection limits were as follows: 1 mg L^{-1} Cl, $50 \mu\text{g L}^{-1}$ Na, Mg, K, and Ca; $40 \mu\text{g L}^{-1}$ Si; $20 \mu\text{g L}^{-1}$ P; $10 \mu\text{g L}^{-1}$ Fe; $1 \mu\text{g L}^{-1}$ Al; $0.5 \mu\text{g L}^{-1}$ Zn; $0.2 \mu\text{g L}^{-1}$ Ni; $0.1 \mu\text{g L}^{-1}$ Cu and Pb; $0.05 \mu\text{g L}^{-1}$ Mn and Cd; and $0.02 \mu\text{g L}^{-1}$ Co.

Fig. 2 Examples of AMW characteristics from Lousal (a), Aljustrel (b), and São Domingos (c). Typical efflorescences sulfates (melanterite) precipitated from AMW after evaporation (d)



The SO_4^{2-} concentrations were determined by ion chromatography in the Geochemistry Laboratory of the Geosciences Department at University of Aveiro, using a Dionex 1000i ion chromatograph and equipped with a Dionex AS4-SC column. An isocratic elution composed of $\text{NaHCO}_3\text{-Na}_2\text{CO}_3$ was used.

The Fe(II)/Fe(III) determinations were carried out by the Ferrozine method according to Viollier et al. (2000), and the measurements were conducted by UV-VIS spectrophotometry (Shimadzu, model UV2101PC) in the Geochemistry Laboratory of the Geosciences Department at University of Aveiro. The Ferrozine reacts with divalent Fe and form stable color indicator, allowing the determination of Fe(II) in solution. By adding a reduction agent (hydroxylamine hydrochloride) to the solution all the Fe(III) was converted to Fe(II) and the Fe_{total} was determined by the same procedure, whereas the Fe(III) was determined by the difference between Fe_{total} and Fe(II). The values of the Fe_{total} obtained by this method were compared with the values of Fe_{total} from the ICP-MS analysis, allowing verified that differences were less than 10%.

Attenuated total reflectance infrared spectroscopy (ATR-IR) analysis was conducted in the non-acidified and unfiltered water samples, using a Bruker Tensor-27 infrared spectrometer equipped with a Ge crystal in a HATR unit, coupled with a temperature regulator from PIKE Technologies. Two reference solutions were obtained from melanterite and CuSO_4 crystals dissolution in water. Both were analyzed to compare the typical

vibration bands of SO_4^{2-} and Me^{n+} and to ascertain the type of metal complexes in AMW.

The zeta potential variation of the AMW was determined for one sample using a Coulter Delsa SX440 equipment. An initial dilution of 1 mL of the water sample was made in 100 mL of a $\text{KCl } 10^{-3} \text{ M}$ ionic solution, followed by a new dilution of 5 mL from this solution in 50 mL of the ionic solution. The pH of the starting point was measured and after that the SC and the zeta potential of the solution were measured in pH intervals, from 2.1 to 10.0, adjusted by HCl or Ca(OH)_2 addition, respectively.

Efflorescences were studied using a high resolution (Schottky) environmental scanning electron microscope (ESEM) FEI Quanta 400 FEG (equipped with a Micro-XRF analyzer, which provides small and micro-spot X-ray analysis and mapping), an energy dispersive spectrometer (EDS) and an electron backscatter diffraction (EBSD) from EDAX Genesis X4M.

Speciation and saturation indices calculations

The species distribution and saturation indices (SI) in AMW samples were calculated by PHREEQC code (version 3.0) (Parkhurst and Appelo 2013), using the thermodynamic WATEQ4F database (Ball and Nordstrom 1991). The solubility simulation of schwertmannite was obtained from the data of Bigham et al. (1996).

The speciation and mineral SI determination include a sequence of steps according to thermodynamic quantities and numerical approximations as described by Nordstrom and Ball (1989) and Alpers and Nordstrom (1999). The SI for each mineral was obtained by comparing measured solution activity, expressed as an ion activity product (IAP) with the theoretical solubility product constant (K_{sp}):

$$SI = \log\left(\frac{IAP}{K_{sp}}\right)$$

$SI > 0$ indicates a supersaturation and the tendency for the mineral phase precipitation, while for $SI < 0$, there is a tendency for dissolution. The $SI = 0$ is indicative of apparent equilibrium between aqueous and solid phases.

Results

Chemistry and physicochemical parameters of acid mine waters

The pH, SC, and the chemical concentrations of the AMW samples studied are shown in Table 1. A negative correlation was found between pH and the total dissolved solids ($r = -0.68$; $\rho < 0.05$). The pH, dilution and evaporation effects, and the proximity to contamination source are the main factors that controlled the amount of metals in waters (e.g., A1 represents a water sample with high heavy metals concentration, obtained from the leached tailings impoundments).

The AMW samples collected close to the tailings impoundments or in open-pits show higher amounts of the total dissolved solids than the AMW samples from streams. The dilution effect in the studied areas is less because the stream flow is intermittent and the evaporation effect is elevated. No significant changes of physicochemical parameters were found during wetting and drying seasons, exception making for sample A6.

The water samples with pH values from 1.7 to 3.5 and high amounts in metals are classified in the Ficklin diagram (Ficklin et al. 1992) (Fig. 3) as acid to high-acid and high-metal to extreme-metal. High variation of metal concentrations and maximum levels were found for Mg, Al, Fe, Cu, Zn, and SO_4 . A positive correlation was found between Al/Fe ($r = 0.89$; $\rho < 0.05$), Al/Cu ($r = 0.98$; $\rho < 0.05$), Al/Zn ($r = 0.91$; $\rho < 0.05$), Al/ SO_4 ($r = 0.98$; $\rho < 0.05$), Fe/Cu ($r = 0.80$; $\rho < 0.05$), Fe/Zn ($r = 0.79$; $\rho < 0.05$), Fe/ SO_4 ($r = 0.86$; $\rho < 0.05$), Cu/Zn ($r = 0.93$; $\rho < 0.05$), Cu/ SO_4 ($r = 0.98$; $\rho < 0.05$), and Zn/ SO_4 ($r = 0.97$; $\rho < 0.05$). The SC values ranging from 1510 to 41,594 $\mu S\ cm^{-1}$ showed a positive correlation with these ions ($0.86 < r < 0.97$; $\rho < 0.05$). Lead showed lower levels than Zn and Cu in the waters, and a

good correlation was found between Pb and K ($r = 0.78$; $\rho < 0.05$).

Metal speciation

Metal species calculation provide a useful information concerning the thermodynamically reactions that can lead to the dissolution or precipitation of mineral phases (Alpers and Nordstrom 1999).

The free metal ion (Me^{n+}) and ion pair between metal and sulfate ($Me-SO_4$) are the dominant species in AMW samples (Fig. 4). A comparison between the Al species and pH (Fig. 5) shows that the $AlSO_4^+$, $Al(SO_4)^{2-}$, and Al^{3+} are the most important species in the pH range of AMW samples. The Al species show a similar trend, well comparable with the Al concentrations in AMW.

The most important Fe species in the pH range 2 to 3.5 is the $FeSO_4^+$, followed by Fe^{3+} , Fe^{2+} , and $FeSO_4^0$ (Fig. 5). The $FeSO_4^+$ and Fe^{3+} show quite similar trends and accompanying the changes in Fe and SO_4 concentrations. Although, at pH greater than 2.3, the dependence on SO_4 concentrations are not so marked for these two species, contrary to Fe^{2+} and $FeSO_4^0$, which show more similarity with SO_4 variations.

The Me^{2+} and $MeSO_4^0$ are the dominant species in AMW samples for Mg, Cu, Zn, and Pb (Fig. 4), where the two species show an equal trend of the Me concentration in AMW (Fig. 5). Magnesium and Zn species also show a similar trend with SO_4 concentrations, and for Cu, this is observed only at pH < 2.2 (Fig. 5). For Pb, the Me^{2+} and $MeSO_4^0$ trends are distinct from SO_4 concentrations (Fig. 5).

The sulfate species formed in the AMW systems provide useful information concerning the precipitation of sulfate minerals, where the toxic metals may co-precipitate or are adsorbed on edge surfaces. In the more acidic AMW samples, the $Fe^{3+}-SO_4^{2-}$ species are dominant, followed by the free ionic SO_4^{2-}/HSO_4^- species, which proportion tends to increase with pH increase. The Al- SO_4 , $MgSO_4^0$, and $CaSO_4^0$ are also important sulfate species of these waters. As a general approach, the Al- SO_4 tends to be higher in lower pH, while $MgSO_4^0$ and $CaSO_4^0$ tend to increase in higher pH conditions (Fig. 6). These general trends own to relative metals concentrations in waters, indicate the precipitation of sulfate minerals (efflorescences) by direct nucleation from AMW.

Molecular complexation of metals in acid mine waters

The molecular behavior of the AMW samples was studied by the ATR-IR technique, because the type of complex plays a key role in the regulation of metal adsorption process and precipitation.

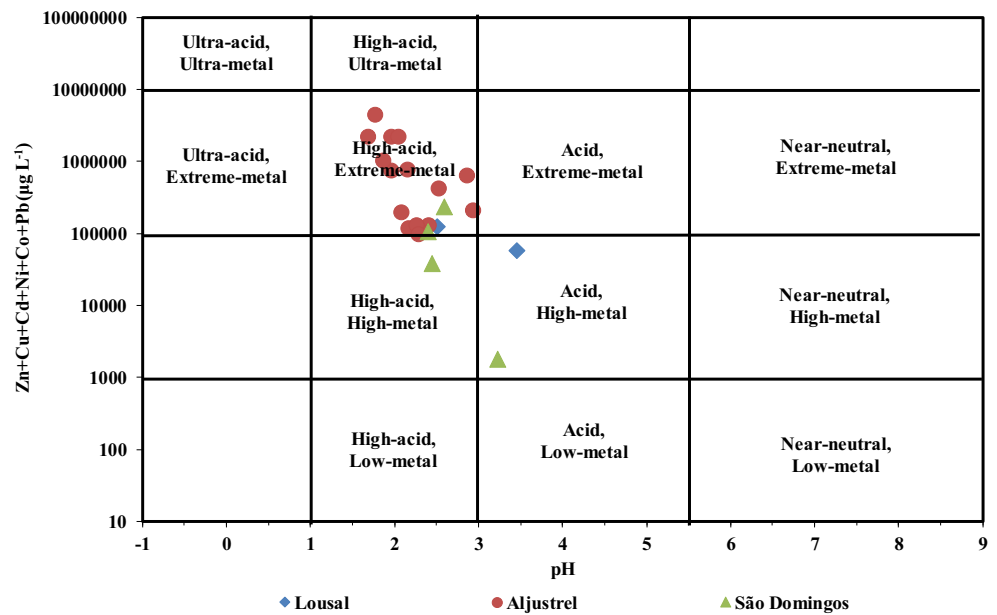
Dissolved melanterite in distilled water (the pH of solution obtained was less than 2) and 1 M $CuSO_4$ solution were used in our ATR-IR experimental measurements (Fig. 7a). The

Table 1 Physicochemical parameters and concentrations of chemical elements and sulfate measurements in the acid mine waters collected from Lousal (L), Aljustrel (A), and São Domingos (SD) mining areas

Sample reference	Sample type	pH	SC μS cm ⁻¹	Na	Mg	Al	Si	P	Cl	K	Ca	Mn	Fe ^(D)	Fe ²⁺	Fe ³⁺	Co	Ni	Cu	Zn	Cd	Pb	SO ₄
L1	OP	3.46	6168	167	697	25	26	0.10	259	16	535	91	3.8	0.9	2.9	2.57	1.08	6	49	0.15	0.21	4041
L2	OP	2.51	10,126	287	1232	57	37	0.10	475	0.25	512	165	571	20	551	4.47	1.73	4	115	0.22	0.004	8179
A1	TI	1.78	41,594	3	4499	8744	56	18	50	3	669	391	840	561	33,762	23.81	9.07	1288	3040	8	0.01	112,911
A2	D	1.97	25,352	69	1888	3458	158	1	158	3	633	323	401	26	10,767	14.93	5.06	755	1423	4	0.13	52,903
A3w	UD	2.87	10,285	178	701	253	21	0.10	407	9	490	243	2.6	329	699	2.81	1.48	21	598	0.99	3	7819
A3d	UD	2.53	10,029	181	1321	97	13	0.10	186	8	411	116	94	116	87	1.29	0.73	17	395	0.46	0.57	9761
A4w	D	2.94	8742	282	676	27	6	1	344	30	666	87	34,323	14	10	0.88	0.49	3	197	0.47	2	6007
A4d	D	2.09	8376	272	577	33	6	2	201	29	741	80	10,793	15	6924	0.86	0.49	9	182	0.47	3	5731
A5w	D	2.41	8154	215	489	3	5	0.75	334	19	687	56	1027	86	1962	0.58	0.30	0.06	123	0.29	2	4553
A5d	D	2.17	6694	206	457	6	5	0.87	183	21	619	53	203	204	617	0.56	0.30	0.55	114	0.28	2	4003
A6w	S	2.05	23,070	89	879	1244	76	1	323	3	588	180	25	57	130	8.33	2.74	333	1857	4	0.04	40,036
A6d	S	1.87	14,585	39	601	1283	64	1	50	3	356	104	6939	2	34	5.80	1.86	287	709	2	0.21	29,431
A7w	S	2.16	10,697	38	342	600	46	0.30	215	0.25	281	76	2048	3	285	2.91	1.22	149	613	1	0.53	7673
A7d	S	1.97	10,992	37	391	749	48	1	50	3	252	66	822	18	471	3.62	1.14	181	563	1	0.08	19,119
A8	S	2.31	4040	138	102	102	19	0.31	229	7	152	11	187	6	4122	0.50	0.17	26	82	0.19	0.06	1926
A9	S	2.27	4298	144	112	140	15	0.82	240	11	122	14	36	28	251	0.65	0.21	33	95	0.22	0.08	2864
A10	S	2.29	4071	148	97	113	12	0.93	265	16	112	10	288	117	5792	0.52	0.17	26	70	0.16	0.01	2372
A11	DT	1.69	36,245	108	1573	3466	101	1	50	169	511	207	489	106	22,638	12.71	3.34	507	1661	5	5	59,776
SD1	OP	2.59	8636	164	733	208	74	0.10	180	4	518	154	4128	4	836	4.19	2.11	70	161	0.96	0.02	7480
SD2	S	2.40	7356	181	361	290	99	0.10	120	2	504	67	279	18	383	2.67	1.26	8	95	0.12	0.27	5442
SD3	S	3.23	1510	95	51	4	6	0.01	130	9	51	6	5909	1.1	1.5	0.06	0.02	0.43	1	0.01	0.002	463
SD4	D	2.45	4804	93	125	236	86	0.10	117	0.77	162	14	22,744	2.5	92	1.36	0.52	23	14	0.06	0.02	2539
Minimum		1.69	1510	3	51	3	5	0.01	50	0.25	51	6	2.6	0.9	2.9	0.06	0.02	0.06	1	0.01	0.002	463
Mean		2.36	12,083	142	814	961	45	1.40	208	16.56	435	114	4189	20	551	4.37	1.61	170.18	553	1.36	0.86	17,956
Maximum		3.46	41,594	287	4499	8744	158	18	475	169	741	391	34,323	561	33,762	23.8	9.1	1288	3040	8	5	112,911
Std. dev.		0.45	10,386	81	959	2006	41	3.80	118	35.08	215	103	8546	26	10,767	5.86	2.06	316.57	776	2.04	1.32	27,059

OP open-pit, TI tailing impoundment, D dam, UD underground mine drainage, S stream, SC specific conductance, AXiv wet season sampling, AXd dry season sampling

Fig. 3 Ficklin diagram (Ficklin et al. 1992) projection of the AMW samples



ATR-IR spectrum of dissolved melanterite is characterized by a strong stretching vibration at 1100 cm^{-1} typical of a *Td* (distorted tetrahedron) SO_4^{2-} symmetry. In the case of CuSO_4 solution (pH ~ 4), the SO_4^{2-} stretching vibration is splitted into two vibration plans (1128 and 1090 cm^{-1}), which confirmed that Cu is sorbed by SO_4^{2-} .

The ATR-IR spectrum of AMW sample L1 (pH 3.5) shows four vibration plans at 1097 , 1118 , 1166 , and 1200 cm^{-1}

(Fig. 7b), which represent the axial deformation of the SO_4 tetrahedron bonded with the Fe-oxyhydroxides (or goethite) and the Me^{n+} sorbed by either SO_4 or Fe-(oxy)hydroxides.

The ATR-IR spectra of the AMW samples SD1 (pH 2.6) and SD4 (pH 2.5) show a vibration plane at 1096 cm^{-1} accompanied by two other plans at 1072 and 1111 cm^{-1} (Fig. 7c). These plans correspond to SO_4 bond to Fe(III) complexes. However, the axial deformation (stretching) assigned

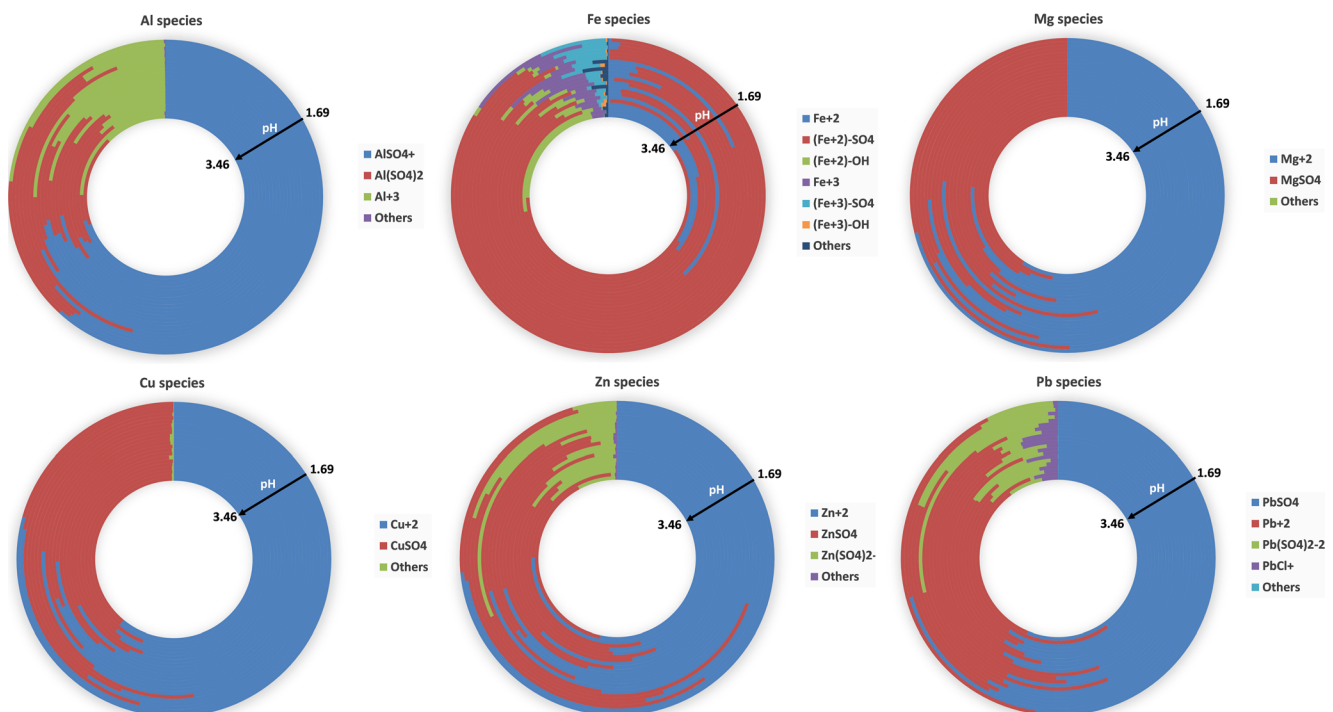


Fig. 4 Percentage distribution of Al, Fe, Mg, Cu, Zn, and Pb species in the AMW samples

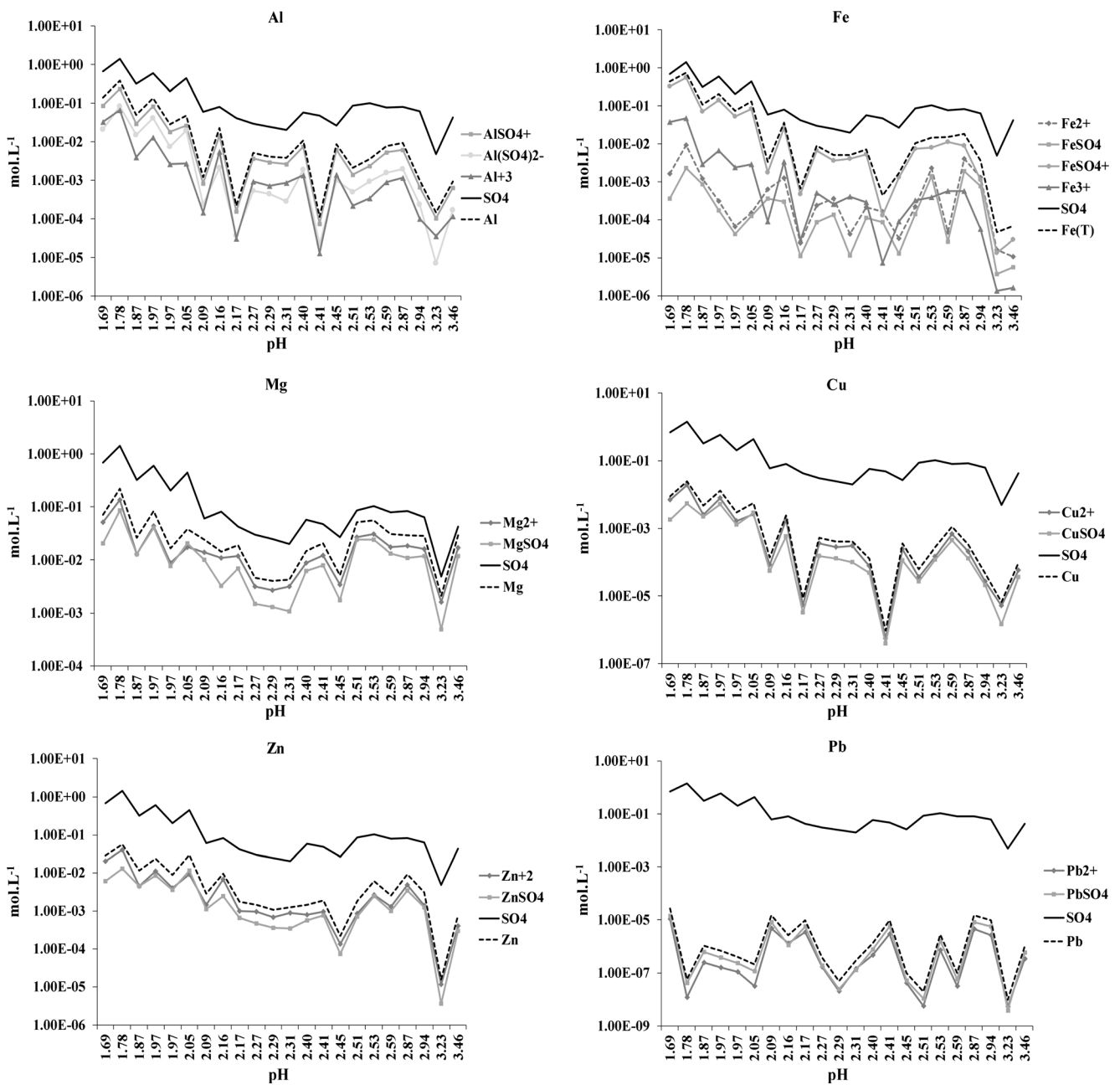


Fig. 5 Distribution of Al, Fe, Mg, Cu, Zn, and Pb concentrations and their dominant species in the AMW samples as a function of pH range and the comparison with SO₄ concentrations

for SO₄ (observed in the case of the dissolved melanterite solution) is accompanied by two vibrations plans.

Zeta potential of acid mine waters

The evolution of the zeta potential and the SC values according to pH variation is shown in Fig. 8. The zeta potential decreases from 23 to 7 mV within the pH range. The stability of zeta potential occurs between the pH values of 3.9 to 5.2 and a slight slope is observed between 5.2 and 8. The SC

decreased rather abruptly when the pH increased from 2.1 to 3.9.

A sequence of pie charts of Fe aqueous species distribution obtained with PHREEQC, according to pH values range, shows that a significant slope of the zeta potential and SC is accompanied by changes of species in the AMW (Fig. 8). The free metal ion (Fe³⁺) and the sulfate species are dominant as pH decreased, while the hydroxide species became dominant in the alkaline pH. The cationic species occur at pH < 7, whereas the anionic species gain relevance at an alkaline pH.

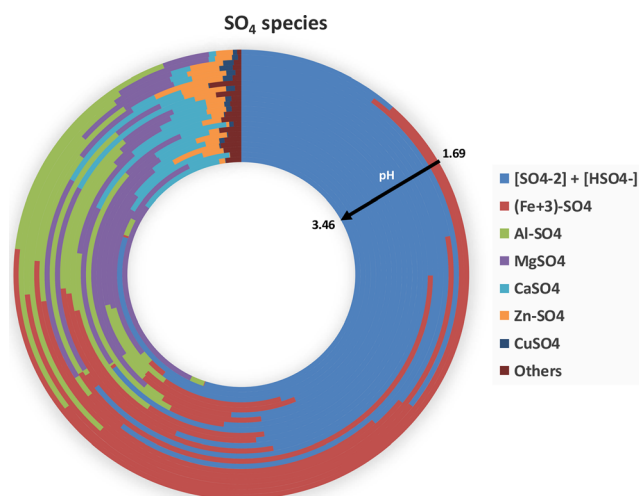


Fig. 6 Percentage distribution of the main sulfate species in AMW samples

Metal precipitation

The SI calculated show that AMW samples were supersaturated ($SI > 0$) in relation to sulfates (namely gypsum), oxyhydroxysulphates (jarosite series and schwertmannite), Fe-(hydr)oxides (e.g., goethite and hematite) and silicates (mainly SiO_2 polymorphs). No Zn species were found to be supersaturated despite their high amounts measured. Cupric ferrite and cuprous ferrite were found supersaturated for the less acidic AMW samples, which are not expected to precipitate due to the low kinetics of these minerals. Also, no Pb species were found supersaturated in AMW samples, with exception of anglesite for two samples showing the high Pb concentrations.

The projection of the SI values of melanterite, epsomite, anglesite, jarosite-K, alunite, goethite, and schwertmannite were compared with the dissolved amounts of Cu, Zn, and Pb. The SI of melanterite, epsomite, and jarosite-K show a slight increase as increasing the dissolved amounts of Cu and Zn in AMW (Fig. 9). No correlation was observed between Pb and the SI of melanterite and epsomite (graphics not shown).

Lead is lesser retained by simple sulfates, but the mixed sulfates or oxy-hydroxysulfates have a tendency for the sorption of Pb (Durães 2011). The SI projection of the jarosite-K against Pb concentrations in AMW samples shows no correlation when the amount of Pb is very low, while a positive correlation is observed when the amount of Pb is greater than 2 mg L^{-1} (Fig. 9). In the case of the highest Pb concentrations, there is a tendency of SI decreasing for jarosite-K, probably caused by the substitutions of K for Pb. Similar behavior was found for alunite (graphic not shown), where Pb can also substitute K (plumboalunite). A good correlation of Pb was found for the SI of anglesite (Fig. 9), where the increase in the

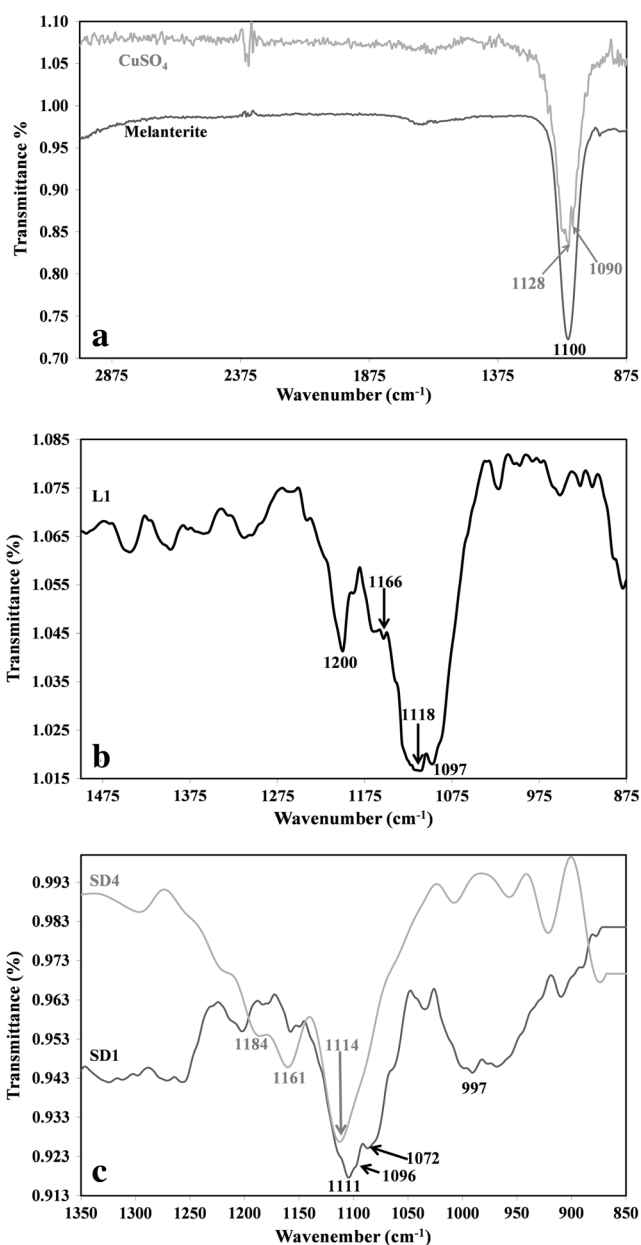


Fig. 7 FTIR-ATR spectra of a dissolved melanterite and a $CuSO_4$ solutions (a), acid water sample L1 (pH 3.5) from Lousal (b), and acid water samples SD1 (pH 2.6) and SD4 (pH 2.5) from São Domingos (c)

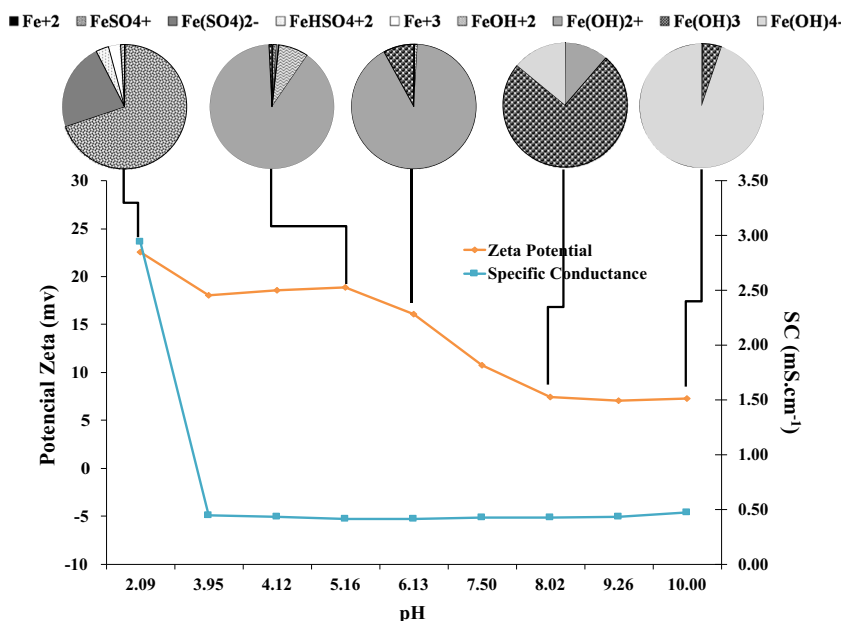
amount of dissolved Pb in waters is accompanied by the SI increase of anglesite (SI closer to the equilibrium).

Goethite and schwertmannite, which are frequently assumed to be good adsorbents of metal(oids) (Bigham and Nordstrom 2000), show a supersaturation in the AMW samples. Although no correlations were found between the amounts of Cu, Zn, and Pb and SI values (graphic not shown).

Efflorescences precipitation—first simple sulfates

Melanterite is one of the first simple sulfates precipitated from AMW. The morphology of melanterite observed at scanning

Fig. 8 Variation of the zeta potential, specific conductance, and Fe species distribution in a AMW sample (sample A2) according to an acid to alkaline pH range



electron microscopy exhibits a pseudo-octahedral, prismatic, or tabular habit (Fig. 10a). Incipient dissolution is characterized by pit-etch and holes observed on the surface planes of melanterite (Fig. 10b). Also, the dehydration process of melanterite is accompanied by its dissolution, generating acid production. Thus, the efflorescent salts are highly soluble and provide an instantaneous source of acidic water upon dissolution and hydrolysis (Nordstrom 1982).

Simple sulfates as melanterite stored rapidly the heavy metals solubilized from AMW during evaporation. Isomorphic substitution of Fe^{2+} for Cu^{2+} or Zn^{2+} may occur during the dehydration—hydration process of melanterite, generating a structural reorganization of the tetrahedral sulfate, well observed by ATR-IR (Fig. 7a). The heavy metals (i.e., Cu^{2+} , Zn^{2+}) from solution trapped in a new structure corresponding either to Zn-(Cu) melanterite or Cu-(Zn) melanterite.

X-ray maps of melanterite corresponding to O, S, and Fe distributions are shown in Fig. 11. Also, X-ray maps of Cu and Zn confirm a distribution of both metals in the melanterite structure (Fig. 11).

Discussion

The AMW samples collected from the Lousal, Aljustrel, and São Domingos mining areas are characterized by extreme low pH values and high amounts of metals (i.e., Mg, Al, Fe, Cu, Zn) and SO_4 , which are responsible for the high SC values. Comparing with the background geochemical levels of the water-type from this region (Ferreira da Silva et al. 2005, 2006, 2009), the following enrichment factors were found:

Al (170–437,200 times), Fe (11–159,000 times), Cu (15–322,000 times), Zn (33–101,333 times), and SO_4 (31–7527 times).

The low Pb amounts in AMW are probably related to its retention by Fe-oxyhydroxides or sulfates, with a greater sorption capacity for Pb than for Cu and Zn in lower pH conditions (Dzombak and Morel 1990; Drever 1997).

Poor correlation was verified between the two sampling periods (wet and dry) in Aljustrel samples due to the exceptional dry year and to the different types of collected samples (e.g., dams, streams). High difference was found for sample A6 affected by dissolution and precipitation cycles and collected near to tailing impoundments.

The speciation calculation indicates that the free ion (Me^{n+}) and the $Me-SO_4$ type species are dominant in AMW conditions (pH 1.7 to 3.5). The cationic sulfate species ($Me^{(3+)}SO_4^+$), in the case of Al and Fe, show the highest concentrations followed by the ion trivalent species (Me^{3+}). The greater expression of Fe^{3+} than Fe^{2+} in high acidity conditions, where the oxidation rate of Fe is lower than its reduction by pyrite, indicates that acidophilic bacteria may mediate this oxidation reaction (Singer and Stumm 1970).

The high SO_4^{2-} concentration in extreme low pH promotes the speciation of Me^{n+} with SO_4^{2-} and the increase of $Me-SO_4$ type species, as reported in previous studies (Monterroso et al. 1994; Shum and Lavkulich 1999). The free ion (Me^{2+}) and the $MeSO_4^0$ type species for Mg, Cu, Zn, and Pb show similar concentrations and trends with a slight domain of Me^{2+} for Mg, Cu, and Zn, whereas the $PbSO_4^0$ concentration is higher in the case of Pb. A dependence on the metal species formed and the SO_4 concentrations was observed, with exception of Pb.

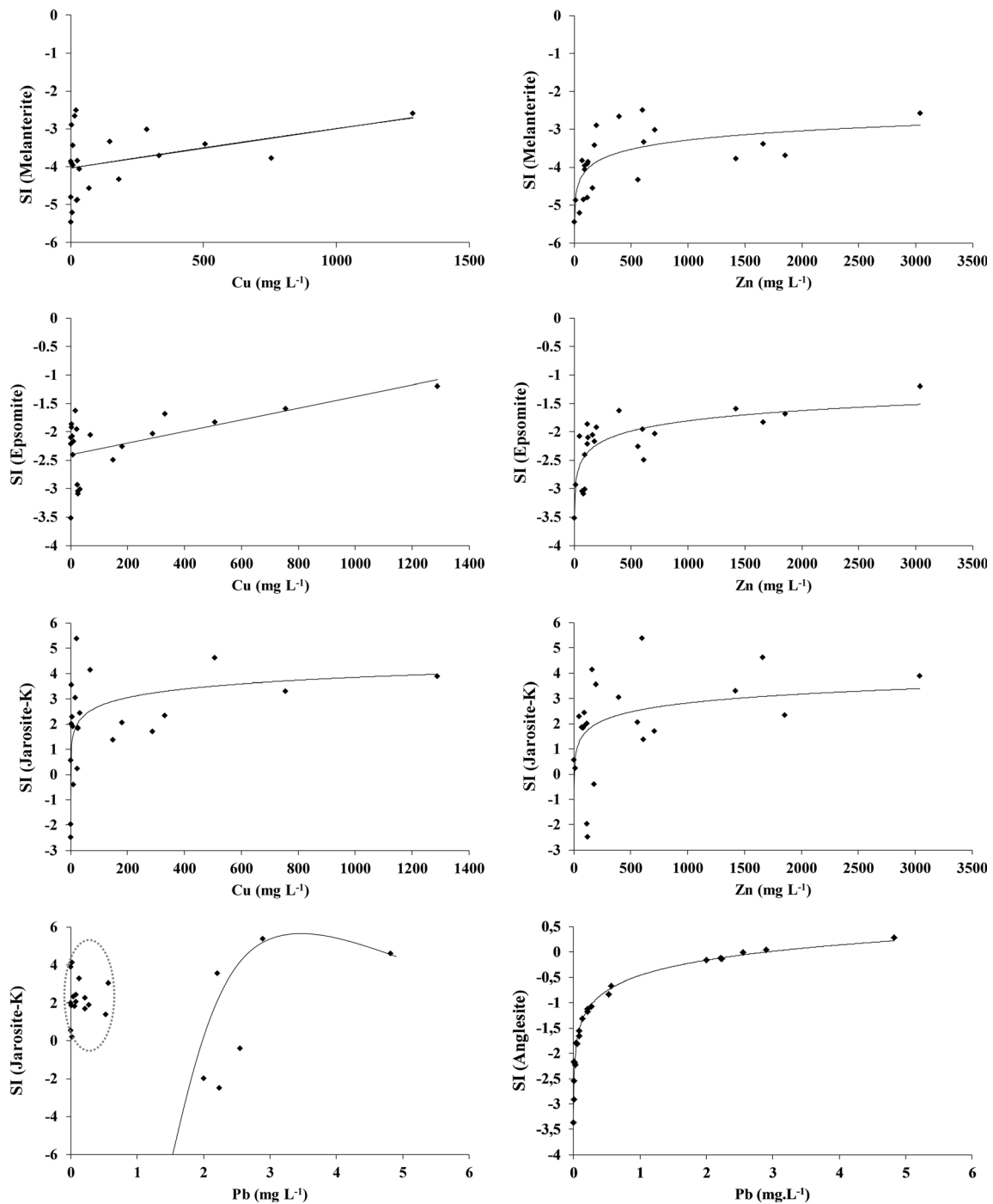


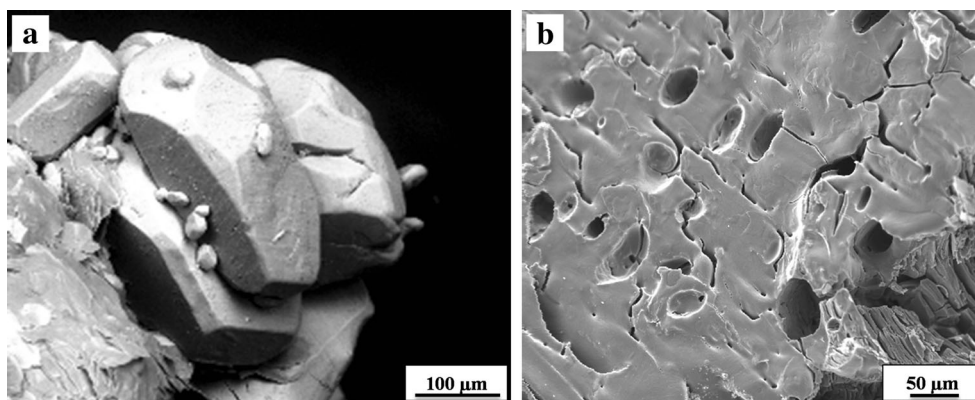
Fig. 9 Saturation indices of melanterite, epsomite, and jarosite-K plotted as a function of Cu and Zn concentrations and saturation indices of jarosite-K and anglesite plotted as a function of Pb concentrations in AMW samples

The distribution of the sulfate species is coincident with the chemical composition of the typical sulfate mineral phases that occur in the studied area (Durães 2011).

The AMW samples analyzed show a very weak chemical bond of the $\text{Me}^{\text{n}+}\text{-S-O-Fe-O}$ with various symmetry configurations (ν_1 , ν_2 , ν_3 , and ν_4). The $\text{Me}^{\text{n}+}$ are adsorbed by either SO_4^{2-} or Fe-oxyhydroxides forming outer- or inner-sphere

complexes. The vibration bands obtained were identified and discussed by Bobos et al. (2006) in AMW from Aljustrel mines, where bands related to SO_4^{2-} and schwertmannite were found (Bishop and Murad 1996). The types of symmetry forming vibration molecular plans of SO_4 caused by metals are detailed described in literature (Hug 1997; Peak et al. 1999; Zhang and Peak 2007).

Fig. 10 Scanning electron microscopy (SEM) photos of melanterite showing the typical morphology (a) and pit-etch and holes on the surface planes (b)



The vibration plans confirm a strong protonation of either SO_4^{2-} and Fe-oxyhydroxides, which formed mono- or bidentate bonds, where monodentate coordination became more relevant with the increase of acidity. This fact may help to explain why in samples with extreme low pH, the Me^{n+} species tends to increase in solution, since the monodentate ligand establish a weaker bond with the metal than a bidentate ligand. Also, sulfate bidentate to monodentate type complexes were also identified in goethite surface with a pH decreasing of AMD (Peretyazhko et al. 2009).

The colloidal particles suspended in waters show different electrical potential, conditioned by different electrical charge of chemical elements. The pH, concentration, and ionic strength of solution influence the complexation type. Large amount of H^+ in solution will compete with metals, favoring the oxyanions adsorption. By contrast, at high pH values and greater number of OH^- in solution, it will favor the competition with anions and the cations adsorption (Dzombak and

Morel 1990; Stumm 1992; Stumm and Morgan 1996; Bigham and Nordstrom 2000). This aspect was observed by zeta potential measurements with pH variation, where significant value variations were accompanied by changes from cationic sulfate to anionic hydroxide type species. The decreasing of SC and zeta potential with pH increasing could be related with the beginning of the colloidal particles aggregation, where metals can be adsorbed regarding the negative charges formed at its surface.

The precipitation of Fe and Mg simple sulfates, gypsum, Fe and Al mixed sulfates, and Fe-hydroxides or oxyhydroxysulfates are the main mineral phases supersaturated in these AMW. During dry periods, the AMW evaporation increases the ionic concentration of these waters and sulfates precipitate. Both Cu and Zn are preferably retained by simple sulfates as melanterite and epsomite. A previous study indicated that epsomite has a greater ability for Zn sequestration than for Cu (Durães 2011).

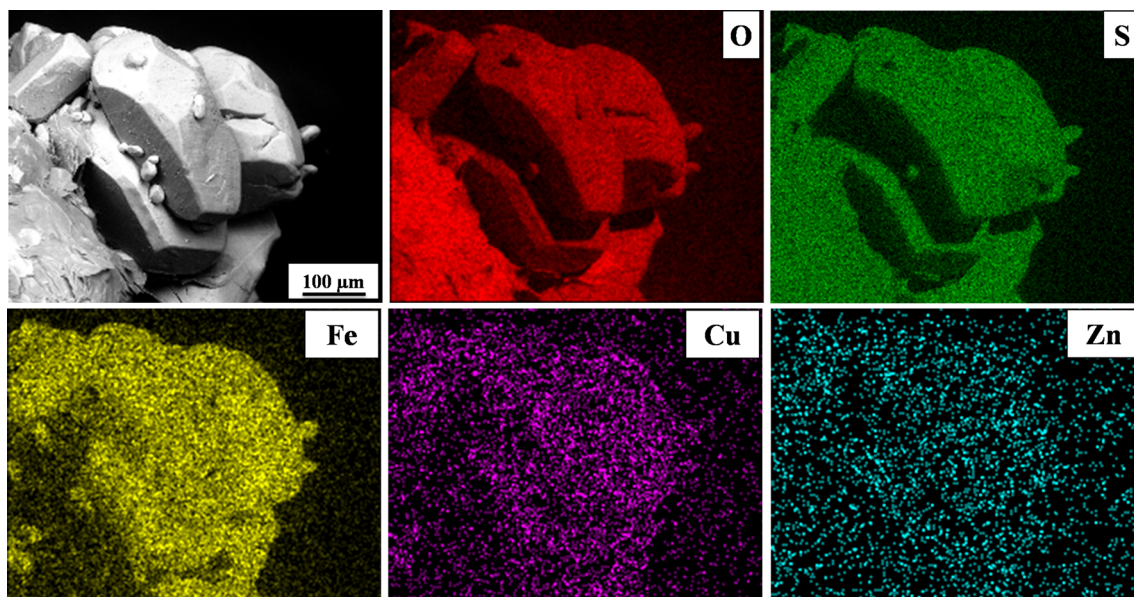


Fig. 11 X-ray element (O, S, Fe, Cu and Zn) distribution maps in melanterite crystals

Lead seems to be more controlled by anglesite precipitation, which is a very insoluble sulfate. Jarosite, which precipitate in high acidic conditions (Bigham et al. 1996; Bigham and Nordstrom 2000), may sequester Pb, forming a mixed K-Pb jarosite, and the same situation may occur with alunite. This is reinforced by the positive correlation between Pb and K identified in AMW samples. Goethite shows a greater stability in a large pH range (Bigham et al. 1996), which it may form surface complexes with metals (e.g., Cu, Zn, Pb). Although in AMW the sorption of heavy metals in goethite or schwertmannite is well-known proved (Bigham and Nordstrom 2000), metal adsorption by sulfates or oxyhydroxysulfates in AMW samples seems to be a more effective process in quantitative terms.

The ATR-IR spectroscopy of AMW enabled the identification of molecular vibration bands corresponding to species theoretically calculated (i.e., Fe^{n+} and SO_4 species) and the molecular complexes formed previously to mineral precipitation after water evaporation. The Me^{n+} were weakly adsorbed by ternary surface complexes (FeOHMeSO_4), confirmed by the crystal-chemistry of melanterite, one of the first phases precipitated after AMW evaporation.

Acknowledgements Nuno Durães is grateful to the Fundação para a Ciência e a Tecnologia (Portugal) for the financial support in the framework of the PhD scholarship (SFRH/BD/22413/2005).

References

- Alpers CN, Nordstrom DK (1999) Geochemical modelling of water-rock interactions in mining environments. In: Plumlee GS, Logsdon MJ (eds) The environmental geochemistry of mineral deposits, part a: processes, methods, and health issues, Rev Econ Geol Vol. 6A. Society of Economic Geology, Littleton, CO, pp. 289–323
- Alpers CN, Nordstrom DK, Thompson JM (1994) Seasonal variations of Zn/Cu ratios in acid mine water from Iron Mountain, California. In: Alpers CN, Blowes DW (eds) Environmental geochemistry of sulfide oxidation, ACS Symp Ser. 550. American Chemical Society, Washington DC, pp. 324–344
- Andrade RFD, Schermerhorn LJG (1971) Aljustrel e Gavião. I Congresso Hispano-Luso-Americano de Geologia Económica, Livro-Guia nº4. Direcção-Geral de Minas e Serviços Geológicos, Lisboa, pp. 32–59
- Ball JW, Nordstrom DK (1991) WATEQ4F-User's manual with revised thermodynamic data base and test cases for calculating speciation of major, trace and redox elements in natural waters. U.S. Geological Survey, Open-File Report 90–129, 185 pp.
- Barriga FJAS (1983) Hydrothermal metamorphism and ore genesis at Aljustrel, Iberian Pyrite Belt. University of Ontario, Canada, Ph.D. Thesis, 368p
- Barriga FJAS, Carvalho D, Ribeiro A (1997) Introduction to the Iberian Pyrite Belt. In: Barriga FJAS, Carvalho D (eds). Geology and VMS deposits of the Iberian Pyrite Belt. Neves Corvo Field Conference, Guidebook Series, Society of Economic Geologists 27:1–20
- Barriga FJAS, Fyfe WS (1988) Giant pyritic base-metal deposits: the example of Feitais (Aljustrel, Portugal). Chem Geol 69(3–4):331–343. doi:10.1016/0009-2541(88)90044-7
- Barriga FJAS, Fyfe WS (1998) Multi-phase water-rhyolite interaction and ore fluid generation at Aljustrel, Portugal. Mineral Deposita 33:88–207. doi:10.1007/s001260050140
- Bigham JM, Nordstrom DK (2000) Iron and aluminium hydroxysulfates from acid sulfate waters. In: Alpers CN, Jambor JL, Nordstrom DK (eds) Sulfate minerals—crystallography, geochemistry, and environmental significance, Rev Mineral Geochem Vol. 40. The Mineralogical Society of America and Geochemical Society, Washington, DC, pp. 351–403
- Bigham JM, Schwertmann U, Traina SJ, Winland RL, Wolf M (1996) Schwertmannite and the chemical modeling of iron in acid sulfate waters. Geochim Cosmochim Acta 60:2111–2121. doi:10.1016/0016-7037(96)00091-9
- Bishop JL, Murad E (1996) Schwertmannite on Mars? Spectroscopic analyses of schwertmannite, its relationship to other ferric minerals, and its possible presence in the surface material of Mars. In: Dyar MD, McCammon C, Schaefer MW (eds) Mineral spectroscopy: a tribute to Roger G. Burns, special publication, vol Vol. 5. Geochemical Society, New York, pp. 337–358
- Bobos I, Durães N, Noronha F (2006) Mineralogy and geochemistry of mill tailings impoundments from Algaes (Aljustrel), Portugal: implications for acid sulphate mine waters formation. J Geochem Explor 88:1–5. doi:10.1016/j.gexplo.2005.08.004
- Carvalho D (1971) Mina de S. Domingos. I Congresso Hispano-Luso-Americano de Geologia Económica, Livro-Guia nº4. Direcção-Geral de Minas e Serviços Geológicos, Lisboa, pp. 59–64
- Carvalho D, Conde L, Enrile JH, Oliveira V, Schermerhorn LJGS (1976) Livro-Guia das excursões geológicas na Faixa Piritosa Ibérica. Comum Serv Geol Port Tomo 60:271–315
- Cravotta CA (2008) Dissolved metals and associated constituents in abandoned coalmine discharges, Pennsylvania, USA. Part 2: geochemical controls on constituent concentrations. Appl Geochem 23(2):203–226. doi:10.1016/j.apgeochem.2007.10.003
- Drever JI (1997) The geochemistry of natural waters: surface and groundwater environments, 3rd edn. Prentice-Hall, Upper Saddle River
- Durães N (2011) Geoquímica dos metais bivalentes tóxicos no sistema solos - sedimentos - águas - plantas em zonas contaminadas áridas e semi-áridas. Ph.D. Thesis, Faculdade de Ciências da Universidade do Porto, 289 pp.
- Dzombak DA, Morel FMM (1990) Surface complexation modelling: hydrous ferric oxide. John Wiley & Sons, New York
- Ferreira da Silva E, Cardoso Fonseca E, Matos JX, Patinha C, Reis P, Santos Oliveira JM (2005) The effect of unconfined mine tailings on the geochemistry of soils, sediments and surface waters of the Lousal area (Iberian Pyrite Belt, southern Portugal). Land Degrad Dev 16:213–228. doi:10.1002/ldr.659
- Ferreira da Silva E, Patinha C, Reis P, Cardoso Fonseca E, Matos JX, Barrosinho J, Santos Oliveira JM (2006) Interaction of acid mine drainage with waters and sediments at the corona stream, Lousal mine (Iberian Pyrite Belt, southern Portugal). Environ Geol 50: 1001–1013. doi:10.1007/s00254-006-0273-6
- Ferreira da Silva E, Bobos I, Matos JX, Patinha C, Reis PA, Cardoso Fonseca E (2009) Mineralogy and geochemistry of trace metals and REE in volcanic massive sulfide host rocks, stream sediments, stream waters and acid mine drainage from the Lousal mine area (Iberian Pyrite Belt, Portugal). Appl Geochem 24:383–401. doi:10.1016/apgeochem.2008.12.001
- Ficklin WH, Plumlee GS, Smith KS, McHugh JB (1992) Geochemical classification of mine drainages and natural drainages in mineralized areas. Proceedings of the 7th International Symposium on Water-Rock Interaction, Balkema, Rotterdam, pp 381–384
- Gaspar O (1996) Microscopia e petrologia de minérios, aplicada à génese, exploração e mineralurgia dos sulfuretos maciços dos jazigos de Aljustrel e Neves Corvo. Est. Notas Trab Inst Geol Min Tomo 38: 3–195

- Hammarstrom JM, Seal RR II, Meier AL, Kornfeld JM (2005) Secondary sulfate minerals associated with acid mine drainage in the eastern US: recycling of metals and acidity in surficial environments. *Chem Geol* 215:407–431. doi:10.1016/j.chemgeo.2004.06.053
- Hug SJ (1997) *In situ* Fourier transform infrared measurements of sulfate adsorption on hematite in aqueous solutions. *J Colloid Interf Sci* 188:415–422. doi:10.1006/jcis.1996.4755
- Jambor JL, Blowes DW (1998) Theory and applications of mineralogy in environmental studies of sulphide-bearing mine wastes. In: Cabril LJ, Vaughan DJ (eds). *Modern approaches to ore and environmental mineralogy*, Short Courses Series Vol. 27, Mineralogical Association of Canada, pp 367–401
- Jambor JL, Nordstrom DK, Alpers CN (2000) Metal-sulfate salts from sulphide mineral oxidation. In: Alpers CN, Jambor JL, Nordstrom DK (eds) *Sulfate minerals—crystallography, geochemistry, and environmental significance*, *Rev Min Geochem* Vol. 40. The Mineralogical Society of America and Geochemical Society, Washington, DC, pp. 303–350
- Janzen MP, Nicholson RV, Scharer JM (2000) Pyrrhotite reaction kinetics: reaction rates for oxidation by oxygen, ferric iron, and for nonoxidative dissolution. *Geochim Cosmochim Acta* 64:1511–1522. doi:10.1016/S0016-7037(99)00421-4
- Jennings SR, Dollhopf DJ, Inskeep WP (2000) Acid production from sulphide minerals using hydrogen peroxide weathering. *Appl Geochem* 15:235–243. doi:10.1016/S0883-2927(99)00041-4
- Jerz JK, Rimstidt JD (2003) Efflorescent iron sulfate minerals: Paragenesis, relative stability, and environmental impact. *Am Mineral* 88:1919–1932
- Kimball BA (1994) Seasonal variation in metal concentrations in a stream affected by acid mine drainage, St. Kevin Gulch, Colorado. In: Filipek LH, Plumlee GS (eds) *The environmental geochemistry of mineral deposits, part B: case studies and research topics*, *Rev Econ Geol* Vol. 6B. Society of Economic Geology, Littleton, CO, pp. 467–477
- Lambert DC, McDonough KM, Dzombak DA (2004) Long-term changes in quality of discharge water from abandoned underground coal mines in Uniontown Syncline, Fayette County, PA, USA. *Water Res* 38(2):277–288. doi:10.1016/j.watres.2003.09.017
- Lottermoser BG (2007) *Mine wastes. Characterization, treatment, environmental impacts*, 2nd edn. Springer-Verlag, Berlin
- Matzke K (1971) *Mina do Lousal. Livro-Guia nº4*. I Congresso Hispano-Luso-Americano de Geologia Económica. Direcção-Geral de Minas e Serviços Geológicos, Lisboa, pp. 25–32
- McCleskey RB (2013) New method for electrical conductivity temperature compensation. *Environ Sci Technol* 47:9874–9881. doi:10.1021/es402188r
- McKibben MA, Tallant BA, del Angel JK (2008) Kinetics of inorganic arsenopyrite oxidation in acidic aqueous solutions. *Appl Geochem* 23:121–135. doi:10.1016/j.apgeochem.2007.10.009
- Millero F (2001) Speciation of metals in natural waters. *Geochem T* 2: 56–64. doi:10.1039/b104809k
- Monterroso C, Alvarez E, Macías F (1994) Speciation and solubility control of Al and Fe in mine soil solutions. *Sci Total Environ* 158: 31–43. doi:10.1016/0048-9697(94)90042-6
- Nicholson RV, Scharer JM (1994) Laboratory studies of pyrrhotite oxidation kinetics. In: Alpers CN, Blowes DW (eds) *Environmental geochemistry of sulfide oxidation*. American Chemical Society Symposium Series, Washington, DC, pp. 14–30
- Nordstrom DK (1982) Aqueous pyrite oxidation and the consequent formation of secondary iron minerals. In: Kittrick JA, Fanning DS, Hossner LR (eds) *Acid sulfate weathering*. Soil Science Society of America, Special Publication 10, Madison, Wisconsin, pp. 37–56
- Nordstrom DK (2009) Acid rock drainage and climate change. *J Geochem Explor* 100:97–104. doi:10.1016/j.gexplo.2008.08.002
- Nordstrom DK (2011) Hydrogeochemical processes governing the origin, transport and fate of major and trace elements from mine wastes and mineralized rock to surface waters. *Appl Geochem* 26:1777–1791. doi:10.1016/j.apgeochem.2011.06.002
- Nordstrom DK, Alpers CN (1999) Geochemistry of acid mine waters. In: Plumlee GS, Logsdon MJ (eds) *The environmental geochemistry of mineral deposits, part a: processes, methods, and health issues*, *Rev Econ Geol* Vol. 6A. Society of Economic Geology, Littleton, CO, pp. 133–160
- Nordstrom DK, Ball JW (1989) Mineral saturation states in natural waters and their sensitivity to thermodynamic and analytical errors. *Sci Géol Bull* 42:269–280
- Oliveira JT, Pereira Z, Carvalho P, Pacheco N, Korn D (2004) Stratigraphy of the tectonically imbricated lithological succession of the Neves Corvo mine area, Iberian Pyrite Belt, Portugal. *Mineral Deposita* 39:422–436. doi:10.1007/s00126-004-0415-2
- Parkhurst DL, Appelo CAJ (2013) Description of input and examples for PHREEQC version 3—A computer program for speciation, batch-reaction, one-dimensional transport, and inverse geochemical calculations: U.S. Geological Survey Water-Resources Investigations. Chapter 43 of Section A, *Groundwater Book 6, Modeling Techniques: Techniques and Methods* 6–A43.
- Peak D, Ford RG, Sparks DL (1999) An *in situ* ATR-FTIR investigation of sulfate bonding mechanisms on goethite. *J Colloid Interf Sci* 218: 289–299. doi:10.1006/jcis.1999.6405
- Peretyazhko T, Zachara JM, Boily J-F, Xia Y, Gassman PL, Arey BW, Burgos WD (2009) Mineralogical transformations controlling acid mine drainage chemistry. *Chem Geol* 262:169–178. doi:10.1016/j.chemgeo.2009.01.017
- Rimstidt JD, Chermak JA, Gagen PM (1994) Rates of reaction of galena, sphalerite, chalcopyrite, and arsenopyrite with Fe(III) in acidic solutions. In: Alpers CN, Blowes DW (eds) *Environmental geochemistry of sulfide oxidation*, ACS Symposium Series 550. American Chemical Society, Washington DC, pp. 2–13
- Romero A, González I, Galán E (2006) The role of efflorescent sulfates in the storage of trace elements in stream waters polluted by acid mine drainage: the case of Peña del Hierro, southwestern Spain. *Can Mineral* 44:1431–1446. doi:10.2113/gscanmin.44.6.1431
- Sánchez España J, López Pamo E, Santofimia E, Aduvire O, Reyes J, Baretino D (2005) Acid mine drainage in the Iberian Pyrite Belt (Odiel river watershed, Huelva, SW Spain): geochemistry, mineralogy and environmental implications. *Appl Geochem* 20:1320–1356. doi:10.1016/j.apgeochem.2005.01.011
- Sánchez España J, López Pamo E, Santofimia Pastor E, Reyes Andrés J, Martín Rubí JA (2006) The removal of dissolved metals by hydroxysulphate precipitates during oxidation and neutralization of acid mine waters, Iberian Pyrite Belt. *Aquat Geochem* 12:269–298. doi:10.1007/s10498-005-6246-7
- Schermerhorn LJG (1971) *A Faixa Piritosa do Sul de Portugal*. I Congresso Hispano-Luso-Americano de Geologia Económica, Livro-Guia nº4. Direcção-Geral de Minas e Serviços Geológicos, Lisboa, pp. 15–25
- Simpson SL, Vardanega CR, Jarolimek C, Jolley DF, Angel BM, Mosley LM (2014) Metal speciation and potential bioavailability changes during discharge and neutralization of acidic drainage water. *Chemosphere* 103:172–180. doi:10.1016/j.chemosphere.2013.11.059
- Singer PC, Stumm W (1970) Acid mine drainage: the rate-determining step. *Science* 167:1121–1123. doi:10.1126/science.167.3921.1121
- Shum M, Lavkulich L (1999) Speciation and solubility relationships of Al, Cu and Fe in solutions associated with sulfuric acid leached mine waste rock. *Environ Geol* 38:59–68. doi:10.1007/s002540050401
- Stumm W (1992) *Chemistry of the solid-water interface: processes at the mineral-water and particle-water interface in natural systems*. John Wiley & Sons, New York

- Stumm W, Morgan J (1996) Aquatic chemistry: chemical equilibria and rates in natural waters, 3rd edn. John Wiley and Sons, New York
- Viollier E, Inglett PW, Hunter K, Roychoudhury AN, Van Cappellen P (2000) The ferrozine method revisited: Fe(II)/Fe(III) determination in natural waters. *Appl Geochem* 15:785–790. doi:[10.1016/S0883-2927\(99\)00097-9](https://doi.org/10.1016/S0883-2927(99)00097-9)
- Walker FP, Schreibe ME, Rimstidt JD (2006) Kinetics of arsenopyrite oxidative dissolution by oxygen. *Geochim Cosmochim Acta* 70:1668–1676. doi:[10.1016/j.gca.2005.12.010](https://doi.org/10.1016/j.gca.2005.12.010)
- Webb JS (1958) Observations on the geology and origin of the San Domingos pyrite deposit, Portugal. *Comun Serv Geol Port* 42:129–143
- Weisener CG, Smart RSC, Gerson AR (2004) A comparison of the kinetics and mechanism of acid leaching of sphalerite containing low and high concentrations of iron. *Int J Miner Process* 74:239–249. doi:[10.1016/S0016-7037\(02\)01276-0](https://doi.org/10.1016/S0016-7037(02)01276-0)
- Yunmei Y, Yongxuan Z, Zheinmin G, Christopher HG, Denxian L (2007) Rates of arsenopyrite oxidation by oxygen and Fe(III) at pH 1.8 – 12.6 and 15 – 45 °C. *Envir Sci Tech* 41:6460–6464. doi:[10.1021/es070788m](https://doi.org/10.1021/es070788m)
- Zhang GY, Peak D (2007) Studies of Cd(II)-sulfate interactions at the goethite-water interface by ATR-FTIR spectroscopy. *Geochim Cosmochim Acta* 71:2158–2169. doi:[10.1016/j.gca.2006.12.020](https://doi.org/10.1016/j.gca.2006.12.020)